

Ab initio Path Integral Monte Carlo Results for the Dynamic Structure Factor of Correlated Electrons: From the Electron Liquid to Warm Dense Matter

T. Dornheim,¹ S. Groth,¹ J. Vorberger,² and M. Bonitz¹

¹*Institut für Theoretische Physik und Astrophysik, Christian-Albrechts-Universität zu Kiel, Leibnizstraße 15, D-24098 Kiel, Germany*

²*Helmholtz-Zentrum Dresden-Rossendorf, D-01328 Dresden, Germany*



(Received 31 October 2018; published 17 December 2018)

The accurate description of electrons at extreme density and temperature is of paramount importance for, e.g., the understanding of astrophysical objects and inertial confinement fusion. In this context, the dynamic structure factor $S(\mathbf{q}, \omega)$ constitutes a key quantity as it is directly measured in x-ray Thomson scattering experiments and governs transport properties like the dynamic conductivity. In this work, we present the first *ab initio* results for $S(\mathbf{q}, \omega)$ by carrying out extensive path integral Monte Carlo simulations and developing a new method for the required analytic continuation, which is based on the stochastic sampling of the dynamic local field correction $G(\mathbf{q}, \omega)$. In addition, we find that the so-called static approximation constitutes a promising opportunity to obtain high-quality data for $S(\mathbf{q}, \omega)$ over substantial parts of the warm dense matter regime.

DOI: 10.1103/PhysRevLett.121.255001

Over the recent years, there has been a remarkable spark of interest in so-called warm dense matter (WDM), an extreme state with high densities ($r_s = \bar{a}/a_B \sim 1$, \bar{a} is the mean interparticle distance and a_B the Bohr radius) and temperatures [$\theta = k_B T/E_F \sim 1$, with $E_F = \hbar^2 q_F^2/2m$ and $q_F = (9\pi/4)^{1/3} a_B/r_s$ being the Fermi energy and wave number]. These conditions occur, for example, in astrophysical objects such as white and brown dwarfs [1–5] and giant planet interiors [6–10], hot-electron chemistry [11,12], laser-excited solids [13], and along the compression path in inertial confinement fusion experiments [14–17]. WDM is nowadays routinely realized at large research facilities like NIF [18,19], LCLS [20,21], and the European X-FEL [22]. Here x-ray Thomson scattering (XRTS) [23–25] has emerged as an important method of diagnostics, with the electronic dynamic structure factor $S(\mathbf{q}, \omega)$ being the central quantity. However, to make XRTS a reliable tool, an accurate theoretical description of the dynamic density response of warm dense electrons is indispensable [26].

In this Letter, we focus on the uniform electron gas (UEG), one of the most fundamental model systems in physics and quantum chemistry [27,28]. While the static properties of the UEG in the ground state have mostly been known for over three decades [29–32], the intricate interplay of Coulomb coupling and quantum degeneracy effects with thermal excitations has rendered a thermodynamic description in the warm dense regime a challenging problem that has only been solved recently [33–35], see Ref. [36] for an extensive review. Naturally, *dynamic* simulations of electrons that are required for frequency-resolved properties

(dynamic conductivity, optical absorption, collective excitations, etc.) and rigorously take into account all the aforementioned effects are even more difficult. Therefore, results for $S(\mathbf{q}, \omega)$ at WDM conditions that go beyond the random phase approximation (RPA) [37] are sparse and have been obtained using uncontrolled approximations, such as diagram-summation-based Green function techniques [38–41]. On the other hand, *ab initio* path integral Monte Carlo (PIMC) [42] simulations can provide an exact description, but are limited to static properties that can be formulated in terms of an “imaginary time,” $i\tau \in [0, i\hbar\beta]$. Therefore, to obtain quantities that depend on frequency, such as $S(\mathbf{q}, \omega)$, one has to perform an analytic continuation from imaginary to real times. Unfortunately, this constitutes a notoriously difficult problem [43–45], and a universal approach is missing.

In this work, we overcome this difficulty for the case of the UEG. (i) We carry out PIMC calculations of the imaginary-time density–density correlation function $F(\mathbf{q}, \tau)$ [see Eq. (1)] for different temperatures $\theta = 0.75, 1, 2, 4$, going from the WDM regime ($r_s = 2$) to the strongly correlated electron liquid ($r_s = 10$). (ii) These data serve as the main input for a new reconstruction method that is based on a stochastic sampling of the dynamic local field correction (LFC) $G(\mathbf{q}, \omega)$ [see Eq. (5)], which allows us to satisfy a multitude of exact constraints. (iii) We are thereby able to present the first accurate results for the dynamic structure factor at WDM conditions and to explicitly study the combined impact of quantum diffraction, temperature and correlation effects on the dispersion relation. (iv) We furthermore investigate the static approximation and uncover that it yields highly accurate results in a

broad parameter range. This opens new avenues towards *ab initio* data for $S(\mathbf{q}, \omega)$ at conditions that would otherwise be inaccessible due to the fermion sign problem [46–48].

In addition to being interesting in their own right, we expect our accurate results for $S(\mathbf{q}, \omega)$ of the UEG to be directly useful for, e.g., the interpretation of WDM experiments [26] (e.g., using the Chihara decomposition [49,50]), various density functional theory (DFT) applications [51–55], and quantum hydrodynamics [56]. Dynamic local field corrections are used not only for the calculation of equilibrium properties but are an important input for several nonequilibrium quantities like the stopping power [57,58], for electron-ion energy transfer rates [59], for the electrical and thermal conductivities [60,61], or for collisional absorption of laser energy [62].

Theory.—We carry out fermionic PIMC simulations of the UEG in the canonical ensemble using a variation of the worm algorithm by Boninsegni *et al.* [63,64] to compute the imaginary-time density–density correlation function (we use Hartree atomic units throughout this work)

$$F(\mathbf{q}, \tau) = \frac{1}{N} \langle n_{\mathbf{q}}(\tau) n_{-\mathbf{q}}(0) \rangle, \quad (1)$$

where the Fourier components of the density, $n_{\mathbf{q}}(\tau)$, are evaluated at imaginary times $\tau \in [0, \beta]$ corresponding to the computation of thermodynamic averages (see Refs. [65,66] for details and the Supplemental Material [67] for a graphical depiction). It should be noted that, although PIMC simulations of electrons are afflicted with a severe sign problem [36,46–48], which constitutes the main obstacle in our simulations, a straightforward evaluation of Eq. (1) using the more advanced permutation blocking PIMC (PB-PIMC) and configuration PIMC (CPIMC) methods [82–85] is not yet possible.

Equation (1) is connected to the dynamic structure factor via

$$F(\mathbf{q}, \tau) = \int_{-\infty}^{\infty} d\omega S(\mathbf{q}, \omega) e^{-\tau\omega}, \quad (2)$$

which means that the task at hand is to perform an inverse Laplace transform to solve for $S(\mathbf{q}, \omega)$. We mention that Eq. (2) is directly obtained by replacing the real time argument in the Fourier transform of $S(\mathbf{q}, \omega)$ (i.e., the intermediate scattering function which is not accessible in PIMC) by $-i\tau$. In addition to our PIMC data for $F(\mathbf{q}, \tau)$, it is also possible to obtain exact results for four frequency moments [27,68–70]

$$\langle \omega^k \rangle = \int_{-\infty}^{\infty} d\omega \omega^k S(\mathbf{q}, \omega), \quad k = -1, 0, 1, 3; \quad (3)$$

see Ref. [67] for details. The typical strategy would now be to find a trial function $S_{\text{trial}}(\mathbf{q}, \omega)$, which, when inserted into Eqs. (2) and (3) reproduces the PIMC data within the given

statistical uncertainty. We investigated different approaches, including the genetic evolution of an entire trial population [44] and the application of a deep neural network to *learn* the needed inverse Laplace transform [86]. Unfortunately, the different methods did not converge towards the same solution for $S(\mathbf{q}, \omega)$ in many cases, which means that the information about the dynamic structure factor provided by Eqs. (2) and (3) is not sufficient to determine a unique solution.

To overcome this obstacle, we make use of the fluctuation-dissipation theorem [27,71],

$$S(\mathbf{q}, \omega) = -\frac{\text{Im}\chi(\mathbf{q}, \omega)}{\pi n(1 - e^{-\beta\omega})}, \quad (4)$$

which links $S(\mathbf{q}, \omega)$ to the imaginary part of the density response function,

$$\chi(\mathbf{q}, \omega) = \frac{\chi_0(\mathbf{q}, \omega)}{1 - v_q[1 - G(\mathbf{q}, \omega)]\chi_0(\mathbf{q}, \omega)}, \quad (5)$$

with $v_q = 4\pi/q^2$, and $\chi_0(\mathbf{q}, \omega)$ referring to the noninteracting system. The dynamic LFC $G(\mathbf{q}, \omega) \in \mathbb{C}$ contains all exchange-correlation effects beyond the mean field level; i.e., the RPA is recovered by setting $G = 0$.

Thus, the computation of $S(\mathbf{q}, \omega)$ has been reformulated into a quest for $G(\mathbf{q}, \omega)$, which is highly advantageous as many properties of the latter are known. More specifically, we stochastically sample trial solutions $G_{\text{trial}}(\mathbf{q}, \omega)$ that exactly fulfill (i) the Kramers-Kronig relation between $\text{Im}G(\mathbf{q}, \omega)$ and $\text{Re}G(\mathbf{q}, \omega)$, (ii) that $\text{Im}G(\mathbf{q}, \omega)$ [$\text{Re}G(\mathbf{q}, \omega)$] is odd [even] with respect to ω , (iii) the correct high and low frequency limits $\text{Re}G(\mathbf{q}, \infty)$ and $\text{Re}G(\mathbf{q}, 0)$ known from our PIMC data, and (iv) the corresponding limits $\text{Im}G(\mathbf{q}, \infty) = \text{Im}G(\mathbf{q}, 0) = 0$. These $G_{\text{trial}}(\mathbf{q}, \omega)$ are then used to compute the corresponding trial structure factors, $S_{\text{trial}}(\mathbf{q}, \omega)$, which are subsequently plugged into Eqs. (2) and (3) and discarded when they are not in agreement with the PIMC data for $F(\mathbf{q}, \tau)$ and $\langle \omega^k \rangle$.

In contrast to the direct reconstruction of $S(\mathbf{q}, \omega)$, the incorporation of the exact constraints on G leads to a drastic reduction in the space of trial structure factors, and the problem becomes tractable. The final result is then computed as the average over the set of those $S_{\text{trial}}(\mathbf{q}, \omega)$ that reproduce $F(\mathbf{q}, \tau)$ and $\langle \omega^k \rangle$ within the given statistical uncertainty. In addition, this allows us to compute the variance of this set as a measure of the remaining uncertainty; see Ref. [67] for details.

Results.—In Fig. 1, we show our results for $S(\mathbf{q}, \omega)$ obtained for $N = 34$ unpolarized electrons at $\theta = 1$ for different values of r_s . To rule out possible finite-size effects, we have carried out PIMC simulations for larger particle numbers where possible. It turns out that, as in the case of the previously studied static structure factor [34,36,46,72], the only effect of the finite simulation

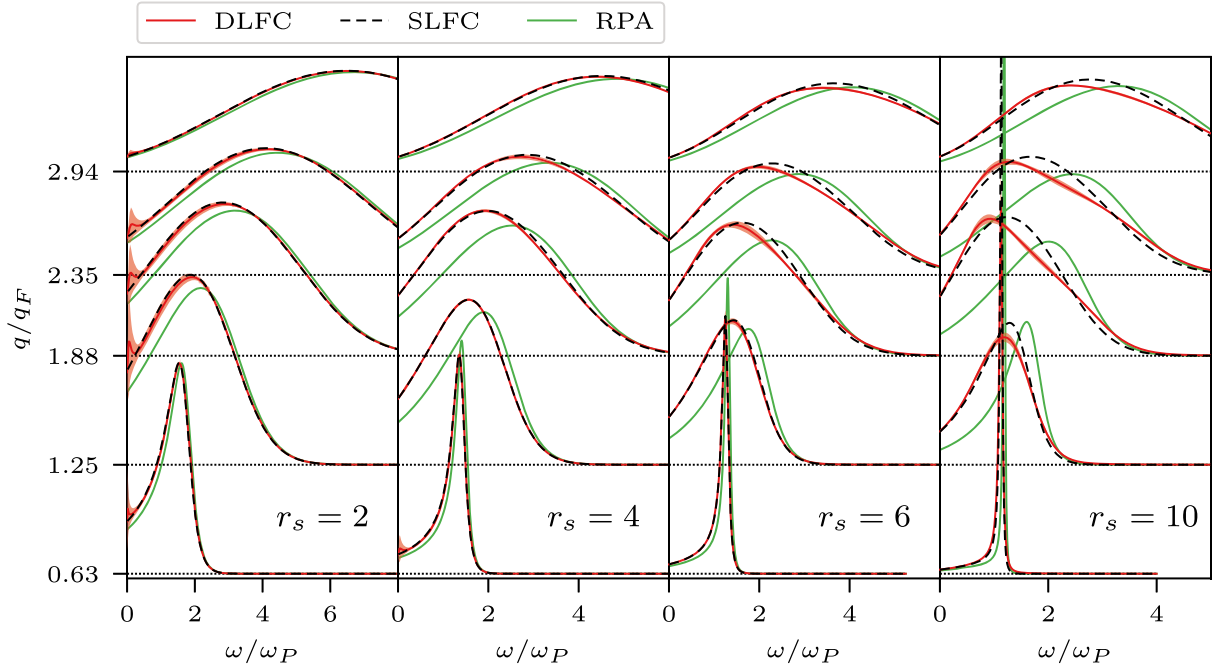


FIG. 1. Dynamic structure factor of the uniform electron gas at $\theta = 1$ for different r_s values. DLFC and SLFC correspond to the full reconstructed dynamic LFC (red) and to using $G_{\text{static}}(\mathbf{q}, \omega) = \text{Re}G(\mathbf{q}, 0)$ (black dashes), respectively. Note that the curves for different r_s have been multiplied with scaling factors. The shaded areas depict the given interval of uncertainty. The coupling strength increases from left to right; the corresponding ratios of mean interaction and kinetic energy are 0.35, 0.79, 1.23, and 2.08, respectively.

box is the discrete set of available \mathbf{q} values, but the functional form of $S(\mathbf{q}, \omega)$ remains practically unchanged. The green curves correspond to the RPA, which exhibits the well-known sharp plasmon peak below a critical wave vector q_c and gets significantly damped upon reaching the pair continuum [27,37], cf. Fig. 2 for the corresponding dispersion relation.

The red curves depict the solutions of our stochastic dynamic LFC (DLFC) procedure. Observe the relatively

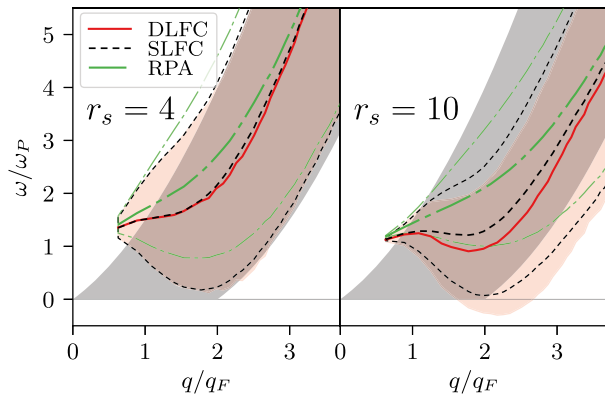


FIG. 2. Peak position (central lines) and full width at half maximum (red shaded area, for DLFC and outer lines, for SLFC and RPA) of $S(q, \omega)$ at $\theta = 1$ for $r_s = 4$ (left) and $r_s = 10$ (right). The shaded gray area indicates the pair continuum in the ground state.

large uncertainty in $S(\mathbf{q}, \omega)$ for $r_s = 2$ at low frequency, which is a direct consequence of the increased statistical uncertainty in $F(\mathbf{q}, \tau)$ caused by the fermion sign problem. This allows for the possibility of a small diffusive peak [87], which is most likely not a real physical effect, but cannot be ruled out on the basis of our PIMC data. Nevertheless, even at this high density, which falls well into the WDM regime, we are able to resolve significant deviations from the RPA around $q = 2q_F$.

With decreasing density, the deviations from the RPA curves become more pronounced, and we observe both a broadening and a significant redshift at intermediate q for $r_s = 4$ and $r_s = 6$. At the strongest coupling strength studied in this work, $r_s = 10$, the DLFC curves, at intermediate q (2.35 and 1.88), develop in addition to the low-frequency maximum, a broad shoulder at higher frequency, close to the peak of the RPA result. This behavior is caused by strong exchange-correlation effects in the dynamic density response and has some resemblance with the ground state results of Takada *et al.* [88,89], where this additional feature was interpreted as an incipient excitonic mode.

Let us now consider the dashed black curves, which correspond to the *static approximation* (SLFC), i.e., to setting $G_{\text{static}}(\mathbf{q}, \omega) = \text{Re}G(\mathbf{q}, 0)$ in Eq. (5). This approach is motivated by the considerable success of static LFC-based schemes such as STLS (Singwi-Tosi-Land-Sjölander) [90–92] and VS (Vashishta-Singwi) [92–94] in the description of the UEG; see Ref. [36] for an extensive topical

discussion. However, in contrast to the approximate treatment of G_{static} in those works, here we use the exact static limit of G that is computed from our PIMC data. The results are striking: evidently, already the inclusion of the exact static LFC leads to an overall very good agreement with the exact results (except for $r_s = 10$) and, thus, to a remarkable improvement over the RPA. At $r_s = 2$, no deviation from the DLFC curve can be resolved within the given accuracy. At $r_s = 4$ and $r_s = 6$, there appear small deviations from the exact result at intermediate q , but both the redshift and the broadening of the peak are reproduced. Even at $r_s = 10$, the static approximation captures the evolution of the plasmon peak, but it misses the broad shoulder at high frequencies.

In Fig. 2, we show the corresponding dispersion relations derived from the peak of $S(\mathbf{q}, \omega)$ for $r_s = 4$ and $r_s = 10$. For the higher density, both the DLFC and SLFC curves exhibit a significant redshift and broadening compared to the RPA for $1 \lesssim q/q_F \lesssim 3$, whereas for small and large wave numbers all three curves eventually converge, as it is expected. Notice the striking agreement between DLFC and the static approximation both in peak position and width over the entire q range.

At $r_s = 10$ the exact dispersion relation exhibits an interesting nonmonotonic behavior with a minimum around $q_{\text{min}} \approx 1.9q_F$, which is in striking contrast to the monotonically increasing RPA curve. The minimum is also visible (although less pronounced) in the static approximation. Such a *negative dispersion* has previously been reported in the ground state both in experiments with alkali metals [95] and in static LFC-based calculations [96,97], as well as in molecular dynamics simulations of the strongly coupled classical one-component plasma [98].

Finally, in Fig. 3, we investigate the temperature dependence of $S(\mathbf{q}, \omega)$ at $r_s = 10$ for $q/q_F \approx 1.88$, i.e., in the minimum of the dispersion relation. At high temperature ($\theta = 4$), DLFC and SLFC are practically indistinguishable whereas the RPA reproduces the broad peak qualitatively. Decreasing the temperature to $\theta = 2$ leads to

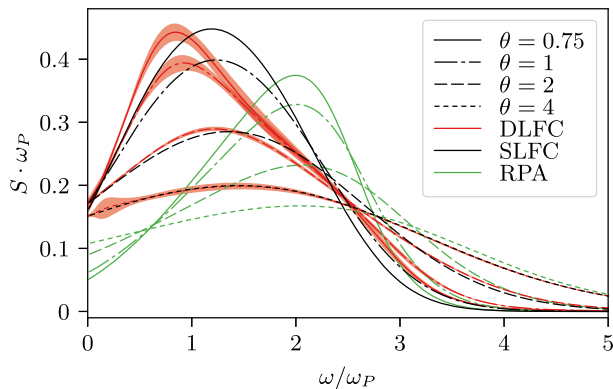


FIG. 3. Dynamic structure factor for $r_s = 10$, $q/q_F \approx 1.88$, and different temperatures that are distinguished by the line styles.

a significantly increased deviation from RPA as the redshift becomes more pronounced. Still, this exchange-correlation effect is almost exactly captured by the static approximation. For the lowest temperatures, $\theta = 1$ and $\theta = 0.75$, the frequency dependence of $G(\mathbf{q}, \omega)$ finally manifests itself, as the red curves exhibit a nontrivial shape with a low-frequency peak and a high-frequency shoulder, which get merged into a single broad peak in the static approximation.

Summary and discussion.—We have carried out PIMC simulations of the UEG from the electron liquid ($r_s = 10$) to the WDM regime ($r_s = 2$) for $0.75 \leq \theta \leq 4$ and computed the imaginary-time density–density correlation function, $F(\mathbf{q}, \tau)$, and various frequency moments, cf. Eq. (3). These data were used as input for our new reconstruction scheme to compute the first *ab initio* data for the dynamic structure factor $S(\mathbf{q}, \omega)$ at finite temperature without any approximation in the treatment of exchange-correlation, temperature, or quantum degeneracy effects. This was achieved by using the fluctuation-dissipation theorem to stochastically sample the dynamic local field correction, $G(\mathbf{q}, \omega)$, fulfilling a multitude of exact properties, which renders the analytic continuation tractable.

This has allowed us to study the impact of correlation effects on $S(\mathbf{q}, \omega)$, which manifest as a small, yet significant broadening and redshift at high density, and an emerging low frequency peak towards stronger coupling. The latter is analogous to a possible incipient excitonic mode previously reported in the ground state [88,89,99]. The application of our approach to even lower densities, $10 < r_s < 100$, to investigate a possible phase transition in the strongly correlated Fermi liquid [89] is beyond the scope of the present work and remains a challenging topic for future research.

In addition to our full dynamic LFC, we have also studied the effect of the static approximation, i.e., by setting $G_{\text{static}}(\mathbf{q}, \omega) = G(\mathbf{q}, 0)$ for all frequencies on $S(\mathbf{q}, \omega)$. The results are very promising, as this approach constitutes a distinct improvement over the RPA for all considered parameters, in particular, in the high density regime, $r_s \lesssim 4$, that is of interest in contemporary WDM research. While the PIMC + DLFC calculations presented in this work are limited by the fermion sign problem, it was recently demonstrated [100,101] that the simulation of the inhomogeneous electron gas using the novel CPIMC and PB-PIMC methods allows for accurate results of the static LFC over significant parts of the WDM regime. Therefore, a future extensive quantum Monte Carlo study of $G(\mathbf{q}, 0)$, which might culminate in a possible parametrization $G(\mathbf{q}, 0; r_s, \theta)$ analogous to previous ground state works [102–104], is highly desirable.

We are confident that our *ab initio* results for the dynamic density response of the UEG will be of high interest for the warm dense matter community and beyond. Direct applications include the interpretation of experiments using XRTS [23] (see Ref. [26] for a topical

discussion), the construction of novel functionals in DFT [51–53] and time-dependent DFT [54], and quantum hydrodynamics [56]. In addition, our data will serve as a valuable benchmark for the development of new methods for the description of the dynamics of warm dense electrons, such as the method of moments by Tkachenko and co-workers [87,105–107] and the recently presented advances in the nonequilibrium Green function method by Kas and Rehr [38,39].

We acknowledge fruitful discussions with H. Kählert and Zh. A. Moldabekov. This work has been supported by the Deutsche Forschungsgemeinschaft via Project No. BO1366-10/2 and by the Norddeutscher Verbund für Hoch- und Höchstleistungsrechnen (HLRN) via Grant No. shp00015 for CPU time.

T. D. and S. G. contributed equally to this work.

-
- [1] D. Saumon, W. B. Hubbard, G. Chabrier, and H. M. van Horn, The role of the molecular-metallic transition of hydrogen in the evolution of Jupiter, Saturn, and brown dwarfs, *Astrophys. J.* **391**, 827 (1992).
- [2] W. B. Hubbard, T. Guillot, J. I. Lunine, A. Burrows, D. Saumon, M. S. Marley, and R. S. Freedman, Liquid metallic hydrogen and the structure of brown dwarfs and giant planets, *Phys. Plasmas* **4**, 2011 (1997).
- [3] G. Chabrier, P. Brassard, G. Fontaine, and D. Saumon, Cooling sequences and color-magnitude diagrams for cool white dwarfs with hydrogen atmospheres, *Astrophys. J.* **543**, 216 (2000).
- [4] A. Becker, W. Lorenzen, J. J. Fortney, N. Nettelmann, M. Schöttler, and R. Redmer, *Ab initio* equations of state for hydrogen (H-REOS.3) and helium (He-REOS.3) and their implications for the interior of brown dwarfs, *Astrophys. J. Suppl. Ser.* **215**, 21 (2014).
- [5] S. H. Glenzer *et al.*, Matter under extreme conditions experiments at the Linac Coherent Light Source, *J. Phys. B* **49**, 092001 (2016).
- [6] J. Vorberger, I. Tamblyn, B. Militzer, and S. A. Bonev, Hydrogen-helium mixtures in the interiors of giant planets, *Phys. Rev. B* **75**, 024206 (2007).
- [7] B. Militzer, W. B. Hubbard, J. Vorberger, I. Tamblyn, and S. A. Bonev, A massive core in Jupiter predicted from first-principles simulations, *Astrophys. J. Lett.* **688**, L45 (2008).
- [8] M. D. Knudson, M. P. Desjarlais, R. W. Lemke, T. R. Mattsson, M. French, N. Nettelmann, and R. Redmer, Probing the Interiors of the Ice Giants: Shock Compression of Water to 700 GPa and 3.8 g/cm³, *Phys. Rev. Lett.* **108**, 091102 (2012).
- [9] F. Soubiran, B. Militzer, K. P. Driver, and S. Zhang, Properties of hydrogen, helium, and silicon dioxide mixtures in giant planet interiors, *Phys. Plasmas* **24**, 041401 (2017).
- [10] M. Schöttler and R. Redmer, *Ab Initio* Calculation of the Miscibility Diagram for Hydrogen-Helium Mixtures, *Phys. Rev. Lett.* **120**, 115703 (2018).
- [11] S. Mukherjee, F. Libisch, N. Large, O. Neumann, L. V. Brown, J. Cheng, J. Britt Lassiter, E. A. Carter, P. Nordlander, and N. J. Halas, Hot electrons do the impossible: Plasmon-induced dissociation of H₂ on Au, *Nano Lett.* **13**, 240 (2013).
- [12] M. L. Brongersma, N. J. Halas, and P. Nordlander, Plasmon-induced hot carrier science and technology, *Nat. Nanotechnol.* **10**, 25 (2015).
- [13] L. Waldecker, R. Bertoni, R. Ernstorfer, and J. Vorberger, Electron-Phonon Coupling and Energy Flow in a Simple Metal Beyond the Two-Temperature Approximation, *Phys. Rev. X* **6**, 021003 (2016).
- [14] R. Nora, W. Theobald, R. Betti, F. J. Marshall, D. T. Michel, W. Seka, B. Yaakobi, M. Lafon, C. Stoeckl, J. Delettrez, A. A. Solodov, A. Casner, C. Reverdin, X. Ribeyre, A. Vallet, J. Peebles, F. N. Beg, and M. S. Wei, Gigabar Spherical Shock Generation on the OMEGA Laser, *Phys. Rev. Lett.* **114**, 045001 (2015).
- [15] P. F. Schmit *et al.*, Understanding Fuel Magnetization and Mix Using Secondary Nuclear Reactions in Magneto-Inertial Fusion, *Phys. Rev. Lett.* **113**, 155004 (2014).
- [16] O. A. Hurricane *et al.*, Inertially confined fusion plasmas dominated by alpha-particle self-heating, *Nat. Phys.* **12**, 800 (2016).
- [17] A. L. Kritcher, T. Döppner, C. Fortmann, T. Ma, O. L. Landen, R. Wallace, and S. H. Glenzer, In-Flight Measurements of Capsule Shell Adiabats in Laser-Driven Implosions, *Phys. Rev. Lett.* **107**, 015002 (2011).
- [18] E. I. Moses, R. N. Boyd, B. A. Remington, C. J. Keane, and R. Al-Ayat, The National Ignition Facility: Ushering in a new age for high energy density science, *Phys. Plasmas* **16**, 041006 (2009).
- [19] B. A. Hammel, S. W. Haan, D. S. Clark, M. J. Edwards, S. H. Langer, M. M. Marinak, M. V. Patel, J. D. Salmonson, and H. A. Scott, High-mode Rayleigh-Taylor growth in NIF ignition capsules, *High Energy Density Phys.* **6**, 171 (2010).
- [20] L. B. Fletcher *et al.*, Ultrabright X-ray laser scattering for dynamic warm dense matter physics, *Nat. Photonics* **9**, 274 (2015).
- [21] P. Sperlberg, E. Gamboa, H. Lee, H. Chung, E. Galtier, Y. Omarbakiyeva, H. Reinholz, G. Röpke, U. Zastra, J. Hastings, L. Fletcher, and S. Glenzer, Free-Electron X-Ray Laser Measurements of Collisional-Damped Plasmons in Isochorically Heated Warm Dense Matter, *Phys. Rev. Lett.* **115**, 115001 (2015).
- [22] T. Tschentscher, C. Bressler, J. Grünert, A. Madsen, A. P. Mancuso, M. Meyer, A. Scherz, H. Sinn, and U. Zastra, Photon beam transport and scientific instruments at the European XFEL, *Appl. Sci.* **7**, 592 (2017).
- [23] S. H. Glenzer and R. Redmer, X-ray Thomson scattering in high energy density plasmas, *Rev. Mod. Phys.* **81**, 1625 (2009).
- [24] J. C. Valenzuela, C. Krauland, D. Mariscal, I. Krasheninnikov, C. Niemann, T. Ma, P. Mabey, G. Gregori, P. Wiewior, A. M. Covington, and F. N. Beg, Measurement of temperature and density using non-collective X-ray Thomson scattering in pulsed power produced warm dense plasmas, *Sci. Rep.* **8**, 8432 (2018).
- [25] J. Vorberger and D. A. Chapman, Quantum theory for the dynamic structure factor in correlated two-component

- systems in nonequilibrium: Application to X-ray scattering, *Phys. Rev. E* **97**, 013203 (2018).
- [26] D. Kraus, B. Bachmann, B. Barbrel, R. W. Falcone, L. B. Fletcher, S. Frydrych, E. J. Gamboa, M. Gauthier, D. O. Gericke, S. H. Glenzer, S. Göde, E. Granados, N. J. Hartley, J. Helfrich, H. J. Lee, B. Nagler, A. Ravasio, W. Schumaker, J. Vorberger, and T. Döppner, Characterizing the ionization depression potential depression in dense carbon plasmas with high-precision spectrally resolved X-ray scattering, *Plasma Phys. Controlled Fusion* **61**, 014015 (2018).
- [27] G. Giuliani and G. Vignale, *Quantum Theory of the Electron Liquid* (Cambridge University Press, New York, 2008).
- [28] P.-F. Loos and P. M. W. Gill, The uniform electron gas, *Comput. Mol. Sci.* **6**, 410 (2016).
- [29] D. M. Ceperley, Ground state of the fermion one-component plasma: A Monte Carlo study in two and three dimensions, *Phys. Rev. B* **18**, 3126 (1978).
- [30] D. M. Ceperley and B. J. Alder, Ground State of the Electron Gas by a Stochastic Method, *Phys. Rev. Lett.* **45**, 566 (1980).
- [31] S. H. Vosko, L. Wilk, and M. Nusair, Accurate spin-dependent electron liquid correlation energies for local spin density calculations: A critical analysis, *Can. J. Phys.* **58**, 1200 (1980).
- [32] J. P. Perdew and A. Zunger, Self-interaction correction to density-functional approximations for many-electron systems, *Phys. Rev. B* **23**, 5048 (1981).
- [33] T. Schoof, S. Groth, J. Vorberger, and M. Bonitz, *Ab Initio* Thermodynamic Results for the Degenerate Electron Gas at Finite Temperature, *Phys. Rev. Lett.* **115**, 130402 (2015).
- [34] T. Dornheim, S. Groth, T. Sjostrom, F. D. Malone, W. M. C. Foulkes, and M. Bonitz, *Ab Initio* Quantum Monte Carlo Simulation of the Warm Dense Electron Gas in the Thermodynamic Limit, *Phys. Rev. Lett.* **117**, 156403 (2016).
- [35] S. Groth, T. Dornheim, T. Sjostrom, F. D. Malone, W. M. C. Foulkes, and M. Bonitz, *Ab Initio* Exchange-Correlation Free Energy of the Uniform Electron Gas at Warm Dense Matter Conditions, *Phys. Rev. Lett.* **119**, 135001 (2017).
- [36] T. Dornheim, S. Groth, and M. Bonitz, The uniform electron gas at warm dense matter conditions, *Phys. Rep.* **744**, 1 (2018).
- [37] D. Pines and P. Nozieres, *Theory of Quantum Liquids* (CRC Press, Boca Raton, Florida, USA, 2018).
- [38] J. J. Kas and J. J. Rehr, Finite Temperature Greens Function Approach for Excited State and Thermodynamic Properties of Cool to Warm Dense Matter, *Phys. Rev. Lett.* **119**, 176403 (2017).
- [39] J. J. Rehr and J. J. Kas, Exchange and correlation in finite-temperature TDDFT, *Eur. Phys. J. B* **91**, 153 (2018).
- [40] T. S. Tan, J. J. Kas, and J. J. Rehr, Coulomb-hole and screened exchange in the electron self-energy at finite temperature, *Phys. Rev. B* **98**, 115125 (2018).
- [41] N.-H. Kwong and M. Bonitz, Real-Time Kadanoff-Baym Approach to Plasma Oscillations in a Correlated Electron Gas, *Phys. Rev. Lett.* **84**, 1768 (2000).
- [42] D. M. Ceperley, Path integrals in the theory of condensed helium, *Rev. Mod. Phys.* **67**, 279 (1995).
- [43] M. Jarrell and J. E. Gubernatis, Bayesian inference and the analytic continuation of imaginary-time quantum Monte Carlo data, *Phys. Rep.* **269**, 133 (1996).
- [44] E. Vitali, M. Rossi, L. Reatto, and D. E. Galli, *Ab initio* low-energy dynamics of superfluid and solid ^4He , *Phys. Rev. B* **82**, 174510 (2010).
- [45] J. Schött, E. G. C. P. van Loon, I. L. M. Locht, M. I. Katsnelson, and I. Di Marco, Comparison between methods of analytical continuation for bosonic functions, *Phys. Rev. B* **94**, 245140 (2016).
- [46] T. Dornheim, S. Groth, F. D. Malone, T. Schoof, T. Sjostrom, W. M. C. Foulkes, and M. Bonitz, *Ab initio* quantum Monte Carlo simulation of the warm dense electron gas, *Phys. Plasmas* **24**, 056303 (2017).
- [47] M. Troyer and U. J. Wiese, Computational Complexity and Fundamental Limitations to Fermionic Quantum Monte Carlo Simulations, *Phys. Rev. Lett.* **94**, 170201 (2005).
- [48] E. Y. Loh, J. E. Gubernatis, R. T. Scalettar, S. R. White, D. J. Scalapino, and R. L. Sugar, Sign problem in the numerical simulation of many-electron systems, *Phys. Rev. B* **41**, 9301 (1990).
- [49] J. Chihara, Difference in X-ray scattering between metallic and non-metallic liquids due to conduction electrons, *J. Phys. F* **17**, 295 (1987).
- [50] J. Chihara, Interaction of photons with plasmas and liquid metals—photoabsorption and scattering, *J. Phys. Condens. Matter* **12**, 231 (2000).
- [51] D. Lu, Evaluation of model exchange-correlation kernels in the adiabatic connection fluctuation-dissipation theorem for inhomogeneous systems, *J. Chem. Phys.* **140**, 18A520 (2014).
- [52] C. E. Patrick and K. S. Thygesen, Adiabatic-connection fluctuation-dissipation DFT for the structural properties of solids—The renormalized ALDA and electron gas kernels, *J. Chem. Phys.* **143**, 102802 (2015).
- [53] A. Pribram-Jones, P. E. Grabowski, and K. Burke, Thermal Density Functional Theory: Time-Dependent Linear Response and Approximate Functionals from the Fluctuation-Dissipation Theorem, *Phys. Rev. Lett.* **116**, 233001 (2016).
- [54] A. D. Baczewski, L. Shulenburger, M. P. Desjarlais, S. B. Hansen, and R. J. Magyar, X-Ray Thomson Scattering in Warm Dense Matter Without the Chihara Decomposition, *Phys. Rev. Lett.* **116**, 115004 (2016).
- [55] E. K. U. Gross and W. Kohn, Local Density-Functional Theory of Frequency-Dependent Linear Response, *Phys. Rev. Lett.* **55**, 2850 (1985).
- [56] Zh. A. Moldabekov, M. Bonitz, and T. S. Ramazanov, Theoretical foundations of quantum hydrodynamics for plasmas, *Phys. Plasmas* **25**, 031903 (2018).
- [57] W. Cayzac *et al.*, Experimental discrimination of ion stopping models near the Bragg peak in highly ionized matter, *Nat. Commun.* **8**, 15693 (2017).
- [58] Z.-G. Fu, Z. Wang, and P. Zhang, Energy loss of α -particle moving in warm dense deuterium plasma: Role of local field corrections, *Phys. Plasmas* **24**, 112710 (2017).

- [59] J. Vorberger, D. O. Gericke, Th. Bornath, and M. Schlanges, Energy relaxation in dense, strongly coupled two-temperature plasmas, *Phys. Rev. E* **81**, 046404 (2010).
- [60] M. P. Desjarlais, P. Michael, C. R. Scullard, L. X. Benedict, H. D. Whitley, and R. Redmer, Density-functional calculations of transport properties in the nondegenerate limit and the role of electron-electron scattering, *Phys. Rev. E* **95**, 033203 (2017).
- [61] M. Veysman, G. Röpke, M. Winkel, and H. Reinholz, Optical conductivity of warm dense matter within a wide frequency range using quantum statistical and kinetic approaches, *Phys. Rev. E* **94**, 013203 (2016).
- [62] P. Hilse, M. Schlanges, T. Bornath, and D. Kremp, Collisional absorption of dense plasmas in strong laser fields: Quantum statistical results and simulation, *Phys. Rev. E* **71**, 056408 (2005).
- [63] M. Boninsegni, N. V. Prokofev, and B. V. Svistunov, Worm algorithm and diagrammatic Monte Carlo: A new approach to continuous-space path integral Monte Carlo simulations, *Phys. Rev. E* **74**, 036701 (2006).
- [64] M. Boninsegni, N. V. Prokofev, and B. V. Svistunov, Worm Algorithm for Continuous-Space Path Integral Monte Carlo Simulations, *Phys. Rev. Lett.* **96**, 070601 (2006).
- [65] D. Thirumalai and B. J. Berne, On the calculation of time correlation functions in quantum systems: Path integral techniques, *J. Chem. Phys.* **79**, 5029 (1983).
- [66] E. Gallicchio and B. J. Berne, The absorption spectrum of the solvated electron in fluid helium by maximum entropy inversion of imaginary time correlation functions from path integral Monte Carlo simulations, *J. Chem. Phys.* **101**, 9909 (1994).
- [67] See Supplemental Material at <http://link.aps.org/supplemental/10.1103/PhysRevLett.121.255001> for detailed information on the utilized sum rules, the parametrization of the dynamic local field correction, and a concise explanation regarding the calculation of uncertainties, which includes Refs. [27,35,36,55,65,66,68–81].
- [68] N. Iwamoto, E. Krotscheck, and D. Pines, Theory of electron liquids. II. Static and dynamic form factors, correlation energy, and plasmon dispersion, *Phys. Rev. B* **29**, 3936 (1984).
- [69] N. Iwamoto, Inequalities for frequency-moment sum rules of electron liquids, *Phys. Rev. A* **33**, 1940 (1986).
- [70] A. A. Kugler, Bounds for some equilibrium properties of an electron gas, *Phys. Rev. A* **1**, 1688 (1970).
- [71] A. A. Kugler, Theory of the local field correction in an electron gas, *J. Stat. Phys.* **12**, 35 (1975).
- [72] T. Dornheim, S. Groth, and M. Bonitz, *Ab initio* results for the static structure factor of the warm dense electron gas, *Contrib. Plasma Phys.* **57**, 468 (2017).
- [73] A. L. Fetter and J. D. Walecka, *Quantum Theory of Many-Particle Systems*, (McGraw-Hill, New York, 1971).
- [74] M. Boninsegni and D. M. Ceperley, Density fluctuations in liquid ^4He . Path integrals and maximum entropy, *J. Low Temp. Phys.* **104**, 339 (1996).
- [75] M. Motta, D. E. Galli, S. Moroni, and E. Vitali, Imaginary time density-density correlations for two-dimensional electron gases at high density, *J. Chem. Phys.* **143**, 164108 (2015).
- [76] G. Sugiyama, C. Bowen, and B. J. Alder, Static dielectric response of charged bosons, *Phys. Rev. B* **46**, 13042 (1992).
- [77] R. D. Puff, Application of sum rules to the low-temperature interacting boson system, *Phys. Rev.* **137**, A406 (1965).
- [78] N. Mihara and R. D. Puff, Liquid structure factor of ground-state He^4 , *Phys. Rev.* **174**, 221 (1968).
- [79] D. Pines and C.-W. Woo, Sum Rules, Structure Factors, and Phonon Dispersion in Liquid ^4He at Long Wavelengths and Low Temperatures, *Phys. Rev. Lett.* **24**, 1044 (1970).
- [80] B. Dabrowski, Dynamical local-field factor in the response function of an electron gas, *Phys. Rev. B* **34**, 4989 (1986).
- [81] A. Meurer *et al.*, SymPy: Symbolic computing in Python, *PeerJ Comput. Sci.* **3**, e103 (2017).
- [82] T. Dornheim, S. Groth, A. Filinov, and M. Bonitz, Permutation blocking path integral Monte Carlo: A highly efficient approach to the simulation of strongly degenerate non-ideal fermions, *New J. Phys.* **17**, 073017 (2015).
- [83] S. Groth, T. Schoof, T. Dornheim, and M. Bonitz, *Ab initio* quantum Monte Carlo simulations of the uniform electron gas without fixed nodes, *Phys. Rev. B* **93**, 085102 (2016).
- [84] T. Dornheim, T. Schoof, S. Groth, A. Filinov, and M. Bonitz, Permutation blocking path integral Monte Carlo approach to the uniform electron gas at finite temperature, *J. Chem. Phys.* **143**, 204101 (2015).
- [85] T. Dornheim, S. Groth, T. Schoof, C. Hann, and M. Bonitz, *Ab initio* quantum Monte Carlo simulations of the uniform electron gas without fixed nodes: The unpolarized case, *Phys. Rev. B* **93**, 205134 (2016).
- [86] T. Dornheim and S. Groth (to be published).
- [87] J. Vorberger, Z. Donko, I. M. Tkachenko, and D. O. Gericke, Dynamic Ion Structure Factor of Warm Dense Matter, *Phys. Rev. Lett.* **109**, 225001 (2012).
- [88] Y. Takada and H. Yasuhara, Dynamical Structure Factor of the Homogeneous Electron Liquid: Its Accurate Shape and the Interpretation of Experiments on Aluminum, *Phys. Rev. Lett.* **89**, 216402 (2002).
- [89] Y. Takada, Emergence of an excitonic collective mode in the dilute electron gas, *Phys. Rev. B* **94**, 245106 (2016).
- [90] K. S. Singwi, M. P. Tosi, R. H. Land, and A. Sjölander, Electron correlations at metallic densities, *Phys. Rev.* **176**, 589 (1968).
- [91] S. Tanaka and S. Ichimaru, Thermodynamics and correlational properties of finite-temperature electron liquids in the Singwi-Tosi-Land-Sjölander approximation, *J. Phys. Soc. Jpn.* **55**, 2278 (1986).
- [92] T. Sjöstrom and J. Dufty, Uniform electron gas at finite temperatures, *Phys. Rev. B* **88**, 115123 (2013).
- [93] P. Vashishta and K. S. Singwi, Electron correlations at metallic densities. V, *Phys. Rev. B* **6**, 875 (1972).
- [94] W. Stolzmann and M. Rösler, Static local-field corrected dielectric and thermodynamic functions, *Contrib. Plasma Phys.* **41**, 203 (2001).
- [95] A. vom Felde, J. Sprösser-Prou, and J. Fink, Valence-electron excitations in the alkali metals, *Phys. Rev. B* **40**, 10181 (1989).
- [96] M. Taut, Plasmon dispersion in the weighted density approximation: Correlation-induced anomaly, *J. Phys. C* **21**, 899 (1988).

- [97] C. Fortmann, A. Wierling, and G. Röpke, Influence of local-field corrections on Thomson scattering in collision-dominated two-component plasmas, *Phys. Rev. E* **81**, 026405 (2010).
- [98] T. Ott, H. Kählert, A. Reynolds, and M. Bonitz, Oscillation Spectrum of a Magnetized Strongly Coupled One-Component Plasma, *Phys. Rev. Lett.* **108**, 255002 (2012).
- [99] M. Higuchi and H. Yasuhara, Kleinman's dielectric function and interband optical absorption strength of simple metals, *J. Phys. Soc. Jpn.* **69**, 2099 (2000).
- [100] T. Dornheim, S. Groth, J. Vorberger, and M. Bonitz, Permutation blocking path integral Monte Carlo approach to the static density response of the warm dense electron gas, *Phys. Rev. E* **96**, 023203 (2017).
- [101] S. Groth, T. Dornheim, and M. Bonitz, Configuration path integral Monte Carlo approach to the static density response of the warm dense electron gas, *J. Chem. Phys.* **147**, 164108 (2017).
- [102] M. Corradini, R. Del Sole, G. Onida, and M. Palumbo, Analytical expressions for the local-field factor $G(q)$ and the exchange-correlation kernel $K_{xc}(r)$ of the homogeneous electron gas, *Phys. Rev. B* **57**, 14569 (1998).
- [103] K. Utsumi and S. Ichimaru, Dielectric formulation of strongly coupled electron liquids at metallic densities. VI. Analytic expression for the local-field correction, *Phys. Rev. A* **26**, 603 (1982).
- [104] B. Farid, V. Heine, G. E. Engel, and I. J. Robertson, Extremal properties of the Harris-Foulkes functional and an improved screening calculation for the electron gas, *Phys. Rev. B* **48**, 11602 (1993).
- [105] Yu. V. Arkhipov, A. Askaruly, D. Ballester, A. E. Davletov, I. M. Tkachenko, and G. Zwicknagel, Dynamic properties of one-component strongly coupled plasmas: The sum-rule approach, *Phys. Rev. E* **81**, 026402 (2010).
- [106] Yu. V. Arkhipov, A. Askaruly, A. E. Davletov, D. Yu. Dubovtsev, Z. Donko, P. Hartmann, I. Korolov, L. Conde, and I. M. Tkachenko, Direct Determination of Dynamic Properties of Coulomb and Yukawa Classical One-Component Plasmas, *Phys. Rev. Lett.* **119**, 045001 (2017).
- [107] Yu. V. Arkhipov, A. B. Ashikbayeva, A. Askaruly, M. Bonitz, L. Conde, A. E. Davletov, T. Dornheim, D. Yu. Dubovtsev, S. Groth, Kh. Santybayev, S. A. Syzganbaeyeva, and I. M. Tkachenko, Sum rules and exact inequalities for strongly-coupled one-component plasmas, *Contrib. Plasma Phys.* **58**, 967 (2018).